Reaction Chemistry & Engineering

ROYAL SOCIETY OF CHEMISTRY

PAPER

View Article Online
View Journal | View Issue

Check for updates

Cite this: *React. Chem. Eng.*, 2025, 10, 686

Structured internals for the intensified Fischer–Tropsch synthesis in fixed-bed reactors†

Evert Boymans, *[a] Yadolah Ganjkhanlou, [a] Marco Denneman,[a] Ben Sutens,[b] Jasper Lefevere[b] and Sander Grootjes[a]

Received 12th November 2024,
Accepted 25th November 2024

DOI: 10.1039/d4re00550c

rsc.li/reaction-engineering

To accelerate the energy transition, processes for the production of sustainable fuels are desired such as the conversion of syngas from biogenic residues into liquid fuel by using the Fischer–Tropsch synthesis (FTS). These novel conversion processes are often of smaller scale due to the feedstock for which intensified reactor concepts are required. Structured reactors present viable alternatives to conventional packed bed reactors. Structured reactors can be obtained by *e.g.* loading a conventional tubular reactor with structured internals. Here, two strategies were followed in an effort to obtain the highest productivity per reactor volume, namely application of 3D-printed catalysts and secondly, thermally conductive aluminium and copper contactors filled with catalyst particles. Superior productivities were obtained by applying Al foam and 3D-printed Cu contactors when packed with FTS catalyst particles, with heat duties of respectively 880 kW m^{-3} and 1238 kW m^{-3} compared with only 185 kW m^{-3} for the 3D-printed catalyst and 218 kW m^{-3} for a conventional packed bed. For the system using the ordered 3D-printed Cu contactors, it presented a productivity of at least 0.85 $g_{C_{5+}}$ g_{cat}^{-1} h^{-1}. The excellent productivities could be correlated to the high thermal conductivity of the metal contactors facilitating the heat transfer from the bed centreline to the reactor wall as revealed by laser flash analysis (LFA) thermal conductivity measurements.

Introduction

As part of the energy transition, the production of sustainable liquid fuels will have to increase significantly in the coming years. Within the EU, the legislative package called Fit-for-55 aims to decrease the total GHG emissions to 55% by 2030. For the aviation sector, the ReFuelEU regulations have been adopted stating a minimum share of sustainable aviation fuel (SAF) starting 2025 (2%) leading to 70% SAF by 2050.[1] In particular, sustainable biobased fuels can play a vital role in meeting the desired quantities according to the RED II.[2] The desired decentralized production of biofuels, *e.g.*, through gasification,[3,4] requires process technology development to ensure high efficiencies at often high flexible operation.

Biogenic residues can be converted to syngas by gasification followed by syngas conversion into liquid fuel by using the Fischer–Tropsch synthesis (FTS) process. In the case of fuels such as diesel or kerosene (middle distillate) production, the highest yield can be obtained by applying low temperature Fischer–Tropsch (LTFT) conditions followed by hydrocracking.[5,6] Generic LTFT conditions are in the range of 200–250 °C and 20–30 bar in 3-phase operation over Co or Fe catalysts.[7] To deal with the high FTS exothermicity of ΔH_r ($C_{10}H_{22}$) = −156 kJ mol_{CO}^{-1}, narrow reactor tubes are applied (<50 mm) cooled by boiling water on the shell side in multi-tube fixed-bed (MTFB) reactors.[7] These reactor tubes contain packed beds of millimeter-sized catalyst pellets. Temperature gradients inside the reactor can be significant, even in the narrow tubes, which can lead to hot spots and thermal runaways. The temperature gradients can be controlled by feed or catalyst dilution or even with non-uniform catalysts[8] but these affect productivity with increasing reactor size as a result. Another solution is the use of structured reactors[9,10] or use of microchannel reactors.[11,12] For obtaining these structured reactors, conventional tubular reactors can be used, modified through the placement of structured internals being either the catalyst itself or conductive contactors filled with a catalyst. When compared to the microchannel reactor, the catalyst loading and unloading is easier in a structured reactor and the maximum loading is higher.[13] Reactor properties such as gas–liquid mixing, convection and conduction can be adjusted in these structured reactors to eventually improve activity and selectivity *i.e.*, productivity

[a] *Netherlands Organisation for Applied Scientific Research – TNO, Westerduinweg 3, 1755 LE Petten, The Netherlands. E-mail: evert.boymans@tno.nl*
[b] *Flemish Institute for Technological Research – VITO, Boeretang 200, B-2400 Mol, Belgium*

† Electronic supplementary information (ESI) available. See DOI: https://doi.org/10.1039/d4re00550c

compared to conventional packed catalyst bed reactors.[9,14] Examples of internals include monoliths with separated parallel channels, corrugated metal sheets, knitted wire (used in distillation) and foams. For loading the catalyst active phase, either the internal itself is catalytically active, the inert wall can be washcoated with a catalyst, or the internal can be filled /packed with catalyst particles.

In recent work, the application of heat conducting structured internals filled with catalyst was found very effective. For instance, Fratalocchi *et al.* have shown that aluminium foams loaded with catalyst particles are particularly effective in controlling the strong exothermicity of the FTS synthesis.[15] They determined the heat duty (Q), which was defined as the released reaction heat per reactor volume, as a measure of productivity. By applying aluminium foam packed with FTS catalyst granules in a 2.78 cm I.D. tubular reactor, heat duties of over 1300 kW m^{-3} were achieved at CO conversions of >65%. They compared this to a conventional packed-bed reactor with diluted catalyst particles, which only reached a maximum productivity of 100 kW m^{-3} before becoming unstable. Moreover, it was concluded that higher productivities can be obtained compared to washcoated structures, which suffer from low catalyst loading.

3D printing offers new developments in the manufacture of structured reactors. An advantage of 3D printing is that it allows for excellent control of the structure geometry, easier catalyst packing, and also potentially improved mixing and heat dissipation compared to conventional packed beds. Examples include the coating of Ni/Al_2O_3 and Ni, $Ru/MgAl_2O_4$ on 3D-printed structures for CO_2 methanation,[16,17] washcoating of the catalyst on printed structures,[18] filling the 3D-printed structure with catalyst particles,[13] or through direct printing of the Ni/Al_2O_3 powder using direct ink writing (DIW), also called robocasting or 3D micro-extrusion.[19] On the latter, in previous work, we have studied 3D-printed structured catalysts and we showed that post impregnation of alumina monoliths is more effective than 3D printing of Co–alumina catalysts for LTFT.[20] However, reports on the use of 3D-printed and ordered porous structures for the FTS are still limited and need reproduction. Moreover, the use of Cu as one of the highly conductive and relatively abundant metals as a heat removal structure inside FTS reactors is not yet well explored.

For this work, as part of the GLAMOUR H2020 project, different structured internals were applied in the FTS in a wall-cooled tubular reactor and their performance compared with that of a conventional packed catalyst bed. In all 4 systems, the composition of the Co-based FTS catalyst is the same. These catalyst systems included a conventional packed bed of a diluted FTS catalyst (packed bed), a 3D-printed structured FTS catalyst (3D Co-cat system), aluminium foam packed with an FTS catalyst (Co-cat//Al-foam) and a 3D-printed Cu internal packed with an FTS catalyst (Co-cat//3D-Cu). For the 3D-printed catalysts, the catalyst itself was prepared through DIW as reported in prior work (referred to as 3D Co-cat).[20] The aluminium foam and 3D-printed Cu internals function as contactors which were then filled with FTS catalyst particles (Co-cat//Al-foam and Co-cat//3D-Cu).

Their maximum FTS productivity in the form of liquid production and heat duty was used as the performance indicator. This maximum was found by slowly increasing the set reactor (wall) temperature up until a thermal runaway occurred, *i.e.*, allowing a thermal runaway to occur. Reactor temperature, syngas conversion and carbon selectivity were carefully monitored during this temperature increase to establish the maximum temperature and productivity under still stable conditions before thermal runaway occurred. Additionally, conductivity measurements were carried out to correlate the catalytic results with the thermal conductivity of the structured catalyst systems.

Materials and methods

The FTS reference catalyst, Co + Ru/γ-Al_2O_3 (12.0% Co, 0.27% Ru) pellets, was obtained in the form of 3 × 3–4 mm cylinders with a BET SA of 189 m^2 g^{-1}, a pore volume of 0.46 mL g^{-1} and a crush strength of 100 N cm^{-2}. Pellets of γ-alumina (>98% purity, BET SA of 220 m^2 g^{-1}) and SiC (>99% purity, BET SA of 30 m^2 g^{-1}) were also obtained as 3 × 3–4 mm cylinders, and were crushed and sieved to the desired particle size range. All three materials were obtained from Riogen, Inc.

The 3D-printed Co + Ru/γ-Al_2O_3 catalyst internals were prepared by DIW of the γ-Al_2O_3 support and performing a Co/Ru impregnation afterwards as described in more detail in previous work[20] and the ESI.†

The aluminum open cell foam (16 pores cm^{-1}, 93% void) was obtained from **http://GoodFellow.com** with dimensions of 150 × 150 × 30 mm from which the cylindrical shaped internals of 30 × 26.1 mm (L × D) were cut using electrical discharge machining.

The 3D-printed Cu internals were 3D-printed through DIW followed by electrical discharge machining to obtain 43.8 × 26.05 (L × D) mm internals. Details on their preparation can be found in previous work[21] and in the ESI.†

Reactor setup

For the catalytic experiments, a tubular fixed bed reactor (wall-cooled) with an internal diameter of 26 mm and a length of 2.5 m was used (Fig. 1). The tubular reactor was then loaded with the different catalyst systems shown in Fig. 2. In each experiment with the different catalyst systems, only a part of the available reactor length was used. A thermal oil flowing through a jacket around the reactor tube (shell side) provides the required heating and cooling of the reactor wall.

The materials used in the different catalyst systems are shown in Fig. 2 with their specific reactor loading shown in Fig. S3.† For the packed bed reference system, the diluted 500–800 μm catalyst provided a catalyst bed length of 620 mm. Also, as seen in Fig. 2, 3D-printed catalysts were applied

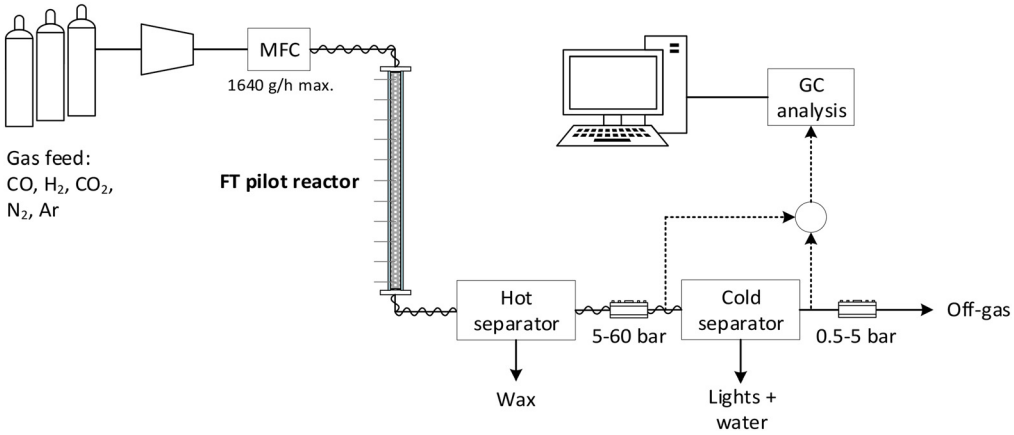

Fig. 1 General flow diagram of the FTS pilot reactor setup.

1. Diluted 500-800 µm FTS catalyst (reference).
2. 3D-printed catalyst (3D Co-cat).
3. Aluminium foam internal
4. 3D-printed Cu internal
Diluted FTS catalyst used to fill Al foam and Cu structure.

Fig. 2 Materials used in all 4 catalyst systems.

for which a total of 8 were placed in the tubular reactor spaced at 240 mm filled with a SiC diluent. Then, an aluminium foam internal can be seen, of which 7 were stacked inside the reactor tube without spacing and filled with the FTS catalyst. Finally, a 3D-printed Cu internal is shown, of which 5 were stacked inside the tubular reactor and filled with the FTS catalyst. These latter two systems will be referred to as respectively Co-cat//Al-foam and Co-cat//3D-Cu. Further details on the reactor and the loading of the reactor with the catalyst systems are provided in the ESI Fig. S2 and S3† and Table S1† therein.

Catalytic experiments

All catalyst systems were activated by introducing 10 vol% H_2 in N_2 at 1 barg at 340 °C (1 °C min^{-1}) for 1 h at an inlet gas flow of 600 g h^{-1}. After activation, the FTS reactor was allowed to cool to 180 °C, ratio control was then set to 63 vol% H_2, 32 vol% CO and 5 vol% Ar at an inlet flow rate of either 500 g h^{-1} (reference and 3D-Co cat) or 200 g h^{-1} (Co-cat//Al-foam and Co-cat//3D-Cu) and the pressure was increased to 20 barg. At this stage, the FTS startup was initiated by setting the heating rate of the thermal oil/reactor wall to 2 °C h^{-1} with a maximum of 250 °C. This gradual temperature increase towards a very high final temperature will be referred to as an FTS startup experiment. The experiment ended when the final temperature was reached, or a thermal runaway occurred beforehand based on a rapid temperature increase inside the catalyst bed detected by one of the thermocouples inside the bed. When runaway occurs, an ESD was automatically triggered, the gas flow stops, and the cooling starts. This is completely automated providing the highest reproducibility. During the experiments, gas samples were continuously withdrawn from the cold separator downstream and analysed by GC to determine the CO conversion, selectivity and productivity.

Conversion X_{CO}, the cobalt-time-yield CTY and carbon selectivity S were calculated based on the following equations:

$$\mathrm{CTY}\left[\mathrm{mol_{CO}\ g_{Co}\ s^{-1}}\right] = \frac{F_{\mathrm{CO,in}} - F_{\mathrm{CO,out}}}{W_{\mathrm{Co}}}$$

$$X_{\mathrm{CO}}\,[\%\mathrm{C}] = \frac{F_{\mathrm{CO,in}} - F_{\mathrm{CO,out}}}{F_{\mathrm{CO,in}}} \cdot 100\%$$

$$S_{\mathrm{C}_n}\,[\%\mathrm{C}] = \frac{F_{\mathrm{C}_n} \times n}{F_{\mathrm{CO,in}} - F_{\mathrm{CO,out}}} \cdot 100\%$$

$$S_{\mathrm{C}_{5+}}\,[\%\mathrm{C}] = 100\% - \sum S_{\mathrm{C}_1\text{–}\mathrm{C4}}$$

where, F_{CO} is the flow of CO in mol h^{-1} and F_{C_n} is the molar carbon flow of component C_n.

The heat duty Q is calculated through:

$$Q\ [\mathrm{kW\ m^{-3}}] = \frac{-\Delta H_r{}^0 \cdot F_{CO,in} \cdot X_{CO}}{V_{cat}}$$

where $\Delta H_r{}^0$ is the standard reaction enthalpy assumed at ΔH_r = −165 kJ $mol_{CO}{}^{-1}$ for the overall FTS reaction, F_{CO} is the molar flow of CO, X_{CO} is the CO conversion divided by the reactor volume occupied by the catalyst V_{cat}. The maximum heat duty (Q_{max}) of a reactor system is based on the maximum CO conversion prior to thermal runaway.

Gas volume is defined in N m^3 under STP conditions. Since 1982, the STP has been defined as a temperature of 273.15 K (0 °C, 32 °F) and an absolute pressure of exactly 105 Pa (100 kPa, 1 bar).[22]

Further information about catalyst characterisation methods is provided in the ESI.†

Results and discussion

Conventionally, the startup of an FTS reactor has to be done very gradually to avoid thermal runaways. In this work, such careful startup was performed by setting all parameters to their desired operational setpoint except the temperature which was set at a low 180 °C. Temperature was then gradually increased to avoid hotspot formation. This startup procedure, as described in detail in the catalytic experiments section, was applied for all the catalyst systems tested in this work. In the absence of suitable heat dissipation, hot spots can still form followed by a thermal runaway much below the desired operational temperature and conversion. Such FTS startup experiments and the maximum productivity before a thermal runaway can serve as a measure for the system's heat dissipation ability.

Fig. 3 illustrates how these FTS startup experiments proceeded for all the 4 catalyst systems. Fig. 3A shows the temperature profiles based on the selected temperatures, being the set wall temperature (measured by the oil inlet) and the highest recorded bed temperature. Fig. 3B–D present the corresponding CO conversion and C_{5+} and C_{CH_4} selectivities as measured by GC. In general, no temperature difference was measured for the thermal oil between the inlet and outlet (see Fig. S4 in the ESI†), meaning that the wall temperature equalled the set oil temperature without temperature gradients in the axial direction.

Conventional packed bed (reference)

Temperature profiles during the FTS startup for the four investigated systems are shown in Fig. 3A. In the case of the conventional packed bed, the reactor wall temperatures (set by the thermal oil on the shell side of the reactor) gradually increased at 2 °C h^{-1} for 13 h as seen in the bottom black line. The second thick black line corresponds to the highest logged temperature inside the catalyst bed. The difference between the wall and bed

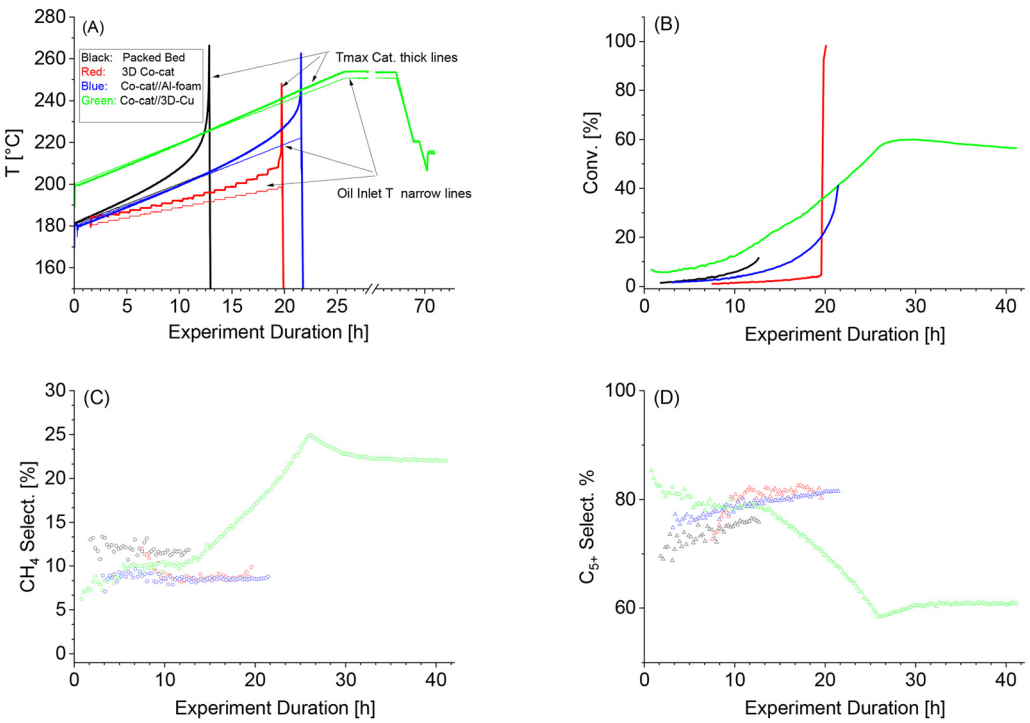

Fig. 3 (A) Temperature profile during the FTS startup for the different catalyst systems. Only the reactor wall temperature (oil inlet) and maximum temperature inside the bed centerline are shown for clarity. (B) The corresponding CO conversions for each system with (C) and (D) the selectivity profiles for respectively CH_4 and C_{5+}. Conditions: gas inlet flow rate of 500 g h^{-1} for the packed bed and 3D Co cat and 200 g h^{-1} for Co-cat//Al-foam and Co-cat//Cu-foam at a composition of 32 vol% CO, 63 vol% H_2, and 5 vol% Ar at 20 barg.

temperature is also referred to as d_{Text}. Following the bed temperature, it shows that initially the temperature is equal to the wall temperature due to a lack of reactivity but starts to deviate from about 190 °C due to increased CO conversion. This continued up to a set temperature of 205 °C, with the temperature difference between wall and centre line (d_{Text}) reaching 15 °C, at which point a thermal runaway occurred, meaning this system could not reach the desired FTS reaction temperature of 220 °C and the accompanied productivities. It is noteworthy that the bed temperatures, monitored by three thermocouples in the centreline showed only a minimal deviation between them, *i.e.*, a minimal axial temperature profile formed (see Fig. S3†). This is because the CO conversion levels are very low up until 200 °C (high flow, low temperature) with no significant concentration gradients from the top to the bottom of the reactor.

Additionally, the CO conversion and selectivities towards CH_4 and C_{5+} are shown in Fig. 3B, C, and D respectively. For the conventional packed bed, in parallel to the bed temperature increase from 180 to 220 °C, the CO conversion increased exponentially to 11.4% at which point the thermal runaway occurred. At this runaway, the CO conversion can easily rise to 100% with substantially higher CH_4 selectivity. This was however not recorded as the emergency shutdown causes the flow to stop. The CH_4 selectivity decreased slightly to around 12%C whereas the C_{5+} selectivity increased slightly from 70%C to 76%C just before the runaway event. We hypothesize that this improved liquid selectivity in time is related to the increased conversion level and the accompanied increase in water partial pressure.[23]

3D Co-cat

In the case of the 3D-printed catalysts, a similar experiment was carried out as also shown by the red lines in Fig. 3A. Surprisingly, an even lower maximum set temperature of 198 °C (and 213 °C at the structure) was achieved when compared to the reference packed bed at a CO conversion of only 4.5%. At this point, the temperature shot up was caused by the formation of hot spots finally resulting in a thermal runaway. The low conversion was the second indication that the heat removal from this system was poor and worse than that of the conventional packed bed. We hypothesize that this could be caused by the lack of diluent within the 3D-printed catalysts resulting in even faster formation of hot spots with an unavoidable thermal runaway at very low conversion. Also, non-optimal wall contact could have played a role; although upon the removal of the catalyst after the experiment, the structures were found to be clamped inside the reactor.

Again, while conversion logically increased with increasing temperature, the C_{5+} and CH_4 selectivity were relatively stable at respectively 80.3%C and 8.9%C as seen in Fig. 3B–D. At the thermal runaway, it can be observed that the CO conversion started to increase exponentially just before the reactor was shut down.

Co-cat//Al-foam

The temperature profile plot during the FTS startup with the aluminium foam can also be seen in Fig. 3A (blue lines). Important considerations for this system were that the catalyst loading density inside the reactor was kept equal to the previous experiments. This was accomplished by dilution with γ-alumina to achieve 0.3 g_{cat} cm^{-3} of reactor volume similar to that applied in the reference and 3D-printed catalyst systems. Furthermore, as the bed length inside the tubular reactor was shorter, the absolute amount of catalyst loaded was lower. To compensate for this, a gas inlet flow of 200 g h^{-1} was applied to maintain a WHSV of 6.5 h^{-1}, again similar to the other applied catalyst systems. Furthermore, in this catalyst system the thermocouple was placed inside the aluminium foam, which is included in Fig. 3A. As can be seen, the d_{Text} remained limited until a set temperature of 222 °C was reached, at which time a thermal runaway occurred due to an exponentially increasing bed temperature as a result of the steeply increasing CO conversion. Similar to the experiments with the prior catalyst systems, the $S_{C_{5+}}$ was relatively constant and actually increasing somewhat, which again was most likely caused by the higher partial pressure of water at higher conversion levels (Fig. 3B–D).[23] At 222 °C, a final $S_{C_{5+}}$ of 82%C was achieved with only 9%C CH_4 at a CO conversion of 41%. This was an excellent result showing the clear benefit of such a conductive structure inside the packed catalyst bed.

Co-cat//3D-Cu

In Fig. 3A, the temperature profiles can also be seen for the 3D-printed Cu contactors packed with catalyst particles (green lines). Again, for comparison with the other systems, a WHSV of 6.5 h^{-1} was maintained. Also, as we expect good heat management, the starting temperature was chosen somewhat higher at 200 °C, but still at a ramp of 2 °C h^{-1}. It can be seen that the d_{Text} remains small with a final value of 3 °C and that the final temperature of 251 °C was reached without any thermal runaway. Both findings illustrate the excellent thermal heat conductivity of the 3D-printed Cu structures even outperforming the aluminium foam structures.

The CO conversion and selectivities can be seen in Fig. 3B–D. As seen, the $S_{C_{5+}}$ remained around 79%C up to a setpoint of 230 °C as can be expected under Co-LTFT conditions, but drops to 61%C at the final temperature of 251 °C. It is to be expected that the selectivity drops at higher temperatures and is the reason why conventionally 220–230 °C is chosen as the operational window. The purpose here is to determine the heat management of the system, which is why the temperature was increased further with an accompanied CO conversion increase to 60% at 251 °C. At the final temperature setpoint of 251 °C, a CO conversion of 60% was achieved, which slightly decreased in the 6 hours after reaching the highest temperature setpoint. This could be related to catalyst deactivation occurring especially under these

more severe conditions. Nonetheless, the GC results confirm that Co-cat//3D-Cu exhibited an excellent heat management allowing to reach high productivity without hot spots or thermal runaways.

An overview of the results with the calculated productivity values for all catalyst systems can be seen in Table 1. The productivity in terms of the liquid production per g catalyst (Y) of the conventional packed bed was 0.17 $g_{C_{5+}}$ g_{cat}^{-1} h^{-1}, which corresponded to a heat duty (Q) of 218 kW m^{-3}.

Comparing this to the structured reactor systems, it shows that the direct 3D-printed catalysts (3D Co-cat) performed worse with a productivity of only 0.09 $g_{C_{5+}}$ g_{cat}^{-1} h^{-1} and a corresponding heat duty of 185 kW m^{-3}. In this case, only a CO conversion of 4.5% was achieved. This poor performance could be explained by a lack of catalyst dilution, the void in the structures and their poor thermal conductivity (further discussed in the next section). Also, the non-ideal contact of the structure with the (cooled) reactor wall cannot be ruled out.

The aluminium foam packed with catalyst particles (Co-cat//Al-foam) performed already much better with a productivity of up to 0.79 $g_{C_{5+}}$ g_{cat}^{-1} h^{-1} and a corresponding heat duty of 880 kW m^{-3} about 4 times better than the conventional packed bed. In order to establish the effect of the flow rate, with this system, the experiment was repeated but at a higher gas inlet flow rate of 500 g h^{-1} (WHSV of 16.3 h^{-1}). Remarkably, increasing the inlet syngas flow rate did not result in a substantial change in maximum productivity, as could be expected from the possible improved heat transfer through convection.

The highest productivity was achieved with the Cu structures (Co-cat//3D-Cu) with a productivity of up to 0.85 $g_{C_{5+}}$ g_{cat}^{-1} h^{-1} and a heat duty (Q) of at least 1238 kW m^{-3}. It is important to note that the calculated heat duty is not the maximum value as a thermal runaway did not occur, and even higher heat duties per m^3 of reactor volume could be achieved. For instance, by loading more catalysts inside the Cu structure *i.e.*, with less diluent. As a result of the higher reactor temperature of 251 °C, the selectivity at this stage was low at an $S_{C_{5+}}$ of only 61%C. Nonetheless, at a similar temperature of 220 °C, the selectivity was also good for Co-cat//3D-Cu at 79%C. Overall, the high heat duty and the absence of thermal runaways of the Cu system establishes its superior heat management allowing *e.g.*, for faster FTS reactor startups and smaller reactors while using less catalyst dilution.

In order to elucidate this phenomenon of improved productivity through improved heat dissipation, the thermal conductivity of all structured catalysts was determined using laser flash analysis (LFA). LFA is a method that uses a light flash for a small period of time (600 μs) and an infrared detector that measures the temperature response on the opposite side of the sample. From the temperature increase and decay, the thermal diffusivity (α), specific heat capacity (C_p) and effective thermal conductivity (k_{eff}) can be determined. To ensure that the heat of the laser was fully absorbed by the structure, the aluminium and copper structures were coated with graphite. The heat transfer through porous materials is complex, as two media are present with the solid phase and the liquid phase in the void. Hence, heat is transferred not only through thermal conduction, but also through convection. Therefore, the heat transfer is described by the effective thermal conductivity, since many factors can contribute to the conductivity in a porous system.

In Table 2, the results are shown for the structures applied in this work, including the 3D-printed catalyst, the aluminium foam and the 3D-printed Cu structure. For the 3D-printed catalyst, the conductivity through the actual catalyst itself is listed. Meanwhile, for the Al and Cu structures, the thermal conductivities are determined in the absence of the actual catalyst particles. These metals are considered inert in the FTS and only facilitate heat transfer. During the LFA measurements, the void for all structures was filled with air. Ranges were reported for the measured values as these were based on heating and cooling stages from 50 to 300 °C.

For the 3D-printed catalyst with a structure density of 0.68 g mL^{-1}, the C_p was determined at 0.5–1.0, which was in the same range as reported elsewhere.[24] The effective thermal conductivity was found to be in the range of 0.1–0.2 W m^{-1} K^{-1}, much lower than that of aluminium oxide (at 10–30 J m^{-1} K^{-1}) attributed to the structure's void and the porosity within the γ-alumina fibres.

The aluminium foam has a very high void of 93%, and hence a low density of 0.24 g mL^{-1}. Nonetheless, an effective thermal conductivity was determined to be in the range of 3.9–4.1 W m^{-1} K^{-1}. This corresponds well with the effective thermal conductivity values reported for similar aluminium foams in the literature.[25,26]

Table 1 Maximum Co-catalysed FTS productivities over different catalyst systems under stable conditions

Catalyst system	Gas flow [g h^{-1}]	T_{wall}/d_{Text}	X_{CO} [%]	$S_{C_{5+}}$ %C	Y [$g_{C_{5+}}$ g_{cat}^{-1} h^{-1}]	Q [kW m^{-3}]
Packed bed	500	205/20	11	76	0.17	218
3D Co-cat	500	198/15	4.5	80	0.09	185
Co-cat//Al-foam	200	222/18	41	82	0.79	880
Co-cat//Al-foam (high flow)	500	222/16	16	81	0.76	860
Co-cat//3D-Cu	200	251/3	60	61/79[b]	0.85	1238[a]

[a] No thermal runaway occurred. [b] Selectivity at 220 °C. Conditions: gas inlet flow rate of 500 g h^{-1} for the packed bed and 3D Co cat and 200 g h^{-1} for Co-cat//Al-foam and Co-cat//Cu-foam at a composition of 32 vol% CO, 63 vol% H_2, and 5 vol% Ar at 20 barg.

Table 2 Result overview from the LFA measurements (in the 50–300 °C range)

Parameter → material	d (structure) [g cm^{-3}]	C_p [J g^{-1} K^{-1}]	α [mm^2 s^{-1}]	k_{eff} [W m^{-1} K^{-1}]
3D-printed catalyst	0.68	0.5–1.0	0.2–0.3	0.1–0.2
Aluminium foam	0.24	0.89	20–22	3.9–4.1
3D-printed Cu internal	2.3	0.1–0.2	35–45	6–16

Furthermore, for the 3D-printed Cu structure, a much higher density of 2.3 g mL^{-1} was determined because of its lower void percentage of 66% and its high intrinsic density. The measured conductivity range was also very high at 6–16 W m^{-1} K^{-1} at a somewhat low C_p value of 0.1–0.2 J g^{-1} K^{-1} (compared to 0.385 J g^{-1} K^{-1}). Clearly, the high intrinsic conductivity of Cu, in combination with the higher density of the Cu structure provided a high conductivity.

When comparing the thermal conductivity with the FTS results, clearly, the Cu and Al structures can successfully transfer/dissipate the heat formed in the FTS to the reactor wall. The conducting metal structures have an effective thermal conductivity much higher than that of the 3D-printed structures. This resulted in much higher (maximum) FTS liquid productivity for systems Co-cat//Al-foam and Co-cat//3D-Cu when compared to the conventional packed bed and 3D Co-cat. For example, the effective conductivity for aluminium was 3.9–4.1 W m^{-1} K^{-1} about 20× higher than the 0.1–0.2 W m^{-1} K^{-1} of the 3D-printed catalyst with the FTS liquid productivities being, respectively, 0.79 and 0.17 $g_{C_{5+}}$ g_{cat}^{-1} h^{-1}, which are 5× higher. The poor performance of the 3D-printed catalyst can thus be correlated to the poor effective thermal conductivity.

Conclusions

The experimental results have shown that the maximum heat duty of the structured 3D-printed catalysts did not exceed that of a conventional packed bed under Co-LTFT conditions. A heat duty (Q) of 185 kW m^{-3} was obtained before a thermal runaway was triggered for the 3D-printed catalyst system compared to a somewhat higher 218 kW m^{-3} for the conventional packed bed.

Conductive contactors of aluminium foam and 3D-printed Cu, packed with catalyst particles, showed superior productivities under Co-LTFT conditions. For the Al foam and 3D-printed Cu catalyst systems, respectively, values of 880 kW m^{-3} and 1238 kW m^{-3} were achieved. These excellent duties provide higher potential productivities of up to 0.85 $g_{C_{5+}}$ g_{cat}^{-1} h^{-1}. This allows us, for example, to load more catalyst per reactor volume or using undiluted syngas at higher pressure, *i.e.*, intensified reactor designs. Moreover, it also provides a more thermally stable system that can be start up and shut down faster without risking thermal runaways, which is especially relevant for dynamic load systems.

Poor heat transfer between the centreline of the catalyst bed and the reactor wall results in hot spot formation and thermal runaway in the highly exothermic FTS. Indeed, thermal conductivity measurements revealed very low conductivities for the 3D-printed catalysts (0.1–0.2 W m^{-1} K^{-1}) *versus* the much higher conductivity for the aluminium foam (3.9–4.1 W m^{-1} K^{-1}) and the 3D-printed Cu contactor (6–16 W m^{-1} K^{-1}). Clearly, the poor performance of the 3D-printed catalyst (and the conventional packed bed) can largely be explained by the poor associated thermal conductivity and thereby heat transfer from the catalyst to the reactor wall. Meanwhile, the metal structures enable sufficient heat transfer through conduction from the centreline to the reactor wall minimizing d_{Text} and improving stability and productivity. In the case of the 3D-printed Cu structure at a set wall temperature of 251 °C, a d_{Text} of only 3 °C was obtained.

Data availability

Data supporting this study are included within the article and/or ESI.† And this study will be published as an open access paper.

Conflicts of interest

There are no conflicts to declare.

Acknowledgements

This research was part of the GLAMOUR project and has received funding from the European Union's Horizon 2020 research and innovation programme under grant agreement No 884197. The authors would like to acknowledge and thank Tom Nijbacker and Michel van der Pal from TNO for their help in carrying out the experimental work presented in this work. Also, the authors would like to thank Bart Michielsen from VITO for his support in the 3D printing development.

References

1 *Fit-for-55 Aviation*, Eur. Parliam. Counc. Eur. UNION, 2021, available at: **https://www.consilium.europa.eu/en/policies/fit-for-55/**.
2 Directive (Eu) 2018/2001 Of The European Parliament And Of The Council, *Off. J. Eur. Union*, 2018, **https://eur-lex.europa.eu/eli/dir/2018/2001/oj**.
3 M. Loewert, J. Hoffmann, P. Piermartini, M. Selinsek, R. Dittmeyer and P. Pfeifer, *Chem. Eng. Technol.*, 2019, **42**, 2202–2214.
4 J. Li, J. Sun, R. Fan, Y. Yoneyama, G. Yang and N. Tsubaki, *ChemCatChem*, 2017, **9**, 2668–2674.
5 S. T. Sie, M. M. G. Senden and H. M. H. Wechem, *Catal. Today*, 1991, **8**, 371–394.

6 A. D. Klerk, *Energy Environ. Sci.*, 2011, **4**, 1177.
7 M. E. Dry, *Catal. Today*, 2002, **71**, 227–241.
8 S. K. Mazidi, M. T. Sadeghi and M. A. Marvast, *Chem. Eng. Technol.*, 2013, **36**, 62–72.
9 K. Pangarkar, T. J. Schildhauer, J. R. Van Ommen, J. Nijenhuis, F. Kapteijn and J. A. Moulijn, *Ind. Eng. Chem. Res.*, 2008, **47**, 3720–3751.
10 Z. Gholami, Z. Tišler and V. Rubáš, *Catal. Rev.: Sci. Eng.*, 2021, **63**, 512–595.
11 L. C. Almeida, F. J. Echave, O. Sanz, M. A. Centeno, G. Arzamendi, L. M. Gandía, E. F. Sousa-Aguiar, J. A. Odriozola and M. Montes, *Chem. Eng. J.*, 2011, **167**, 536–544.
12 R. Myrstad, in *2nd Trondheim Gas Technology Conference*, Trondheim-Norway, 2011.
13 L. Fratalocchi, G. Groppi, C. G. Visconti, L. Lietti and E. Tronconi, *Chem. Eng. J.*, 2020, **386**, 123988.
14 J. A. Moulijn and F. Kapteijn, *Curr. Opin. Chem. Eng.*, 2013, **2**, 346–353.
15 L. Fratalocchi, C. G. Visconti, G. Groppi, L. Lietti and E. Tronconi, *Chem. Eng. J.*, 2018, **349**, 829–837.
16 S. Danaci, L. Protasova, V. Middelkoop, N. Ray, M. Jouve, A. Bengaouer and P. Marty, *React. Chem. Eng.*, 2019, **4**, 1318–1330.
17 M. González-Castaño, F. Baena-Moreno, J. C. N. de Miguel, K. U. M. Miah, F. Arroyo-Torralvo, R. Ossenbrink, J. A. Odriozola, W. Benzinger, A. Hensel, A. Wenka and H. Arellano-García, *Energy Convers. Manage.*, 2022, **258**, 115464.
18 R. Balzarotti, M. Ambrosetti, M. Arnesano, A. Anglani, G. Groppi and E. Tronconi, *Appl. Catal., B*, 2021, **283**, 119651.
19 V. Middelkoop, A. Vamvakeros, D. De Wit, S. D. M. Jacques, S. Danaci, C. Jacquot, Y. De Vos, D. Matras, S. W. T. Price and A. M. Beale, *J. CO2 Util.*, 2019, **33**, 478–487.
20 J. Lefevere, B. Sutens, E. Boymans and B. Michielsen, *Catal. Today*, 2024, 114585.
21 S. Kolli, M. Beretta, A. Selema, P. Sergeant, L. A. I. Kestens, M. Rombouts and J. Vleugels, *Addit. Manuf.*, 2023, **73**, 103670.
22 ISO 13443:1996/Cor 1: 1997 (Natural gas — Standard reference conditions), available at: **https://www.iso.org/standard/20461.html**.
23 S. Storsæter, Ø. Borg, E. A. Blekkan and A. Holmen, *J. Catal.*, 2005, **231**, 405–419.
24 A. Saffar Shamshirgar, M. Belmonte, G. C. Tewari, R. E. Rojas Hernández, J. Seitsonen, R. Ivanov, M. Karppinen, P. Miranzo and I. Hussainova, *Materials*, 2021, **14**, 2242.
25 Y. Amani, A. Takahashi, P. Chantrenne, S. Maruyama, S. Dancette and E. Maire, *Int. J. Heat Mass Transfer*, 2018, **122**, 1–10.
26 R. Dyga and S. Witczak, *Procedia Eng.*, 2012, **42**, 1088–1099.